

# Direct Numerical Simulation of Flow Past a Sphere in a Plane Turbulent Boundary Layer with Immersed Boundary Method

Hui Zhao, Anyang Wei, Kun Luo and Jianren Fan

State Key Laboratory of Clean Energy Utilization, Zhejiang University, Hangzhou, China

**Keywords:** Direct Numerical Simulation, Immersed Boundary Method, Boundary Layer, Sphere, Plane.

**Abstract:** Direct Numerical Simulation coupled with Immersed Boundary Method (IBM) has attracted wide attention recent years, making this technique a significant role in many practical engineering areas. This paper described a direct numerical study of flow past a sphere above a plane, which can obtain detail information of flow field and vortex structure. A combined multiple-direct forcing and immersed boundary method (MDF/IBM) was used to deal with the coupling between fluid and solid. The Reynolds number based on sphere diameter was 4171. Behaviours of the vortices were observed through the simulation. The velocity distribution switched from laminar boundary to turbulent boundary. A recirculation region was observed behind the sphere. The influence of the sphere on the boundary layer, the center peak defect, the turbulence intensity and the Reynolds stresses are explored.

## 1 INTRODUCTION

A number of studies have been carried out on a flow pasting a three-dimensional obstacle placed on the plane boundary, especially the flow past a sphere. Obtaining enough data and understanding the structure of flow field and vortex are extremely necessary. Because from an engineering viewpoint, the spherical structure application can be seen everywhere in practice, such as some structures exposed in the wind, vehicles moving in fluid and so on. After Schlichting studied a blunt obstacle placed on the plane boundary with the effect of surface roughness (Schlichting, 1939), the drag of a sphere placed on a ground plate (Klemin et al., 1939) was investigated. An experimental study of the turbulent shear layer behind a sphere placed on a plane boundary was performed (Okamoto, 1980). The surface pressure distribution on a sphere, the velocity and pressure distribution in the shear layer behind a sphere were measured. It was found that the wall wake behind a sphere became low and spreads transversely with the downstream distance increasing. Takayuki (Takayuki, 2008) investigated the flow around a sphere placed at various heights above a plane boundary. In Takayuki's experimental study, the surface pressure distribution on the sphere and the plane were measured, meanwhile empirical equations of the drag and lift coefficients were defined.

In recent years, with the development of the computer technology, it becomes possible to do research on two-phase flow in turbulent boundary layer using direct numerical simulation method. Fully resolved direct numerical simulations were considered to investigate a turbulent channel flow over an isolated particle of finite size (Zeng et al., 2008) with the spectral element methodology (SEM). To validate a joint application of direct numerical simulation and a combined multiple-direct forcing and immersed boundary method (MDF/IBM), a flow past an isolated three-dimensional hemispherical roughness element mounted on a flat plate was simulated (Zhou et al., 2010). Nevertheless, numerical simulation studies on the interaction between sphere and plane boundary layer are lacking, which could be significant to engineering application.

This paper describes a direct numerical study on the flow field and the vortex structure on a sphere above a plane. The influence of the sphere on the boundary layer is explored, such as velocity distribution, turbulence intensity, Reynolds stresses and vortex structure.

## 2 NUMERICAL METHOD

### 2.1 Governing Equations

In the computational domain  $\Omega$ , the dimensionless governing equations for incompressible viscous flows are:

$$\nabla \cdot \mathbf{u} = 0, \quad (1)$$

$$\frac{\partial \mathbf{u}}{\partial t} + \mathbf{u} \cdot \nabla \mathbf{u} = -\nabla P + \frac{1}{Re} \nabla^2 \mathbf{u} + \mathbf{f}. \quad (2)$$

Here,  $\mathbf{u}$  is the dimensionless velocity of fluid,  $P$  is the dimensionless pressure,  $Re$  is the Reynolds number defined as  $Re = \frac{\rho UL}{\mu}$ , where  $\rho$  is the characteristic density of fluid,  $U$  is the characteristic velocity,  $L$  is the characteristic length of flow field and  $\mu$  is the viscosity of fluid.

### 2.2 Multi-direct Forcing Immersed Boundary Method

Function  $\mathbf{f}$  in the momentum equation (2) is the mutual interaction force between fluid and immersed boundary, this dimensionless external force is expressed as:

$$\mathbf{f}(\mathbf{x}, t) = \int_{\Omega} \mathbf{F}_k(\mathbf{x}_k) \cdot \delta(\mathbf{x} - \mathbf{x}_k) d\mathbf{x}_k, \quad (3)$$

where  $\delta(\mathbf{x} - \mathbf{x}_k)$  is the Dirac-delta function.  $\mathbf{x}_k$  is the position of the  $k$ th Lagrangian point on the immersed boundary.  $\mathbf{x}$  is the position of the Eulerian grid nodes.  $\mathbf{F}_k(\mathbf{x}_k)$  is the force that exerts on the fluid by the  $k$ th Lagrangian point of the immersed boundary.

$$\begin{aligned} \mathbf{F}_k(\mathbf{x}_k) &= \frac{\mathbf{u}_k^{n+1} - \mathbf{u}_k^n}{\Delta t} \\ &\quad - \left( \mathbf{u} \cdot \nabla \mathbf{u} + \nabla P \right. \\ &\quad \left. - \frac{1}{Re} \nabla^2 \mathbf{u} \right) \\ &= \frac{\hat{\mathbf{u}}_k^{n+1} - \hat{\mathbf{u}}_k^n}{\Delta t} - \frac{\hat{\mathbf{u}}_k - \mathbf{u}_k^n}{\Delta t} \\ &\quad - \mathbf{rhs}, \end{aligned} \quad (4)$$

where  $\mathbf{rhs} = -(\mathbf{u} \cdot \nabla \mathbf{u} + \nabla P - \frac{1}{Re} \nabla^2 \mathbf{u})$ , and  $n, n+1$  represent two different time.

Here,  $\hat{\mathbf{u}}_k$  is an intermediate variable which satisfies the governing equations of the pure flow field, then we can get  $\frac{\hat{\mathbf{u}}_k - \mathbf{u}_k^n}{\Delta t} - \mathbf{rhs} = 0$ .

In order to ensure that the no-slip boundary condition of the velocity at the immersed boundary

could be satisfied, Direct forcing (Mohd-Yusof, 1997) is introduced to make the velocity on the Lagrangian points approaching the velocity of the no-slip boundary. Therefore the force exerted on the  $k$ th Lagrangian point at the immersed boundary is:

$$\mathbf{F}_k(\mathbf{x}_k) = \frac{\mathbf{u}_k^{n+1} - \hat{\mathbf{u}}_k}{\Delta t} = \frac{\mathbf{u}_L - \hat{\mathbf{u}}_k}{\Delta t}. \quad (5)$$

If this direct forcing is exerted by  $l+1$  times, the intermediate velocity  $\hat{\mathbf{u}}_k$  could be much closer to the desired velocity  $\mathbf{u}_L$ . Then  $\mathbf{F}_k(\mathbf{x}_k)$  could be expressed as:

$$\mathbf{F}_k^{l+1}(\mathbf{x}_k) = \frac{\mathbf{u}_L - \hat{\mathbf{u}}_k^l}{\Delta t}. \quad (6)$$

At the same time, to spread the force from the Lagrangian points to the Eulerian grids, the two way coupling between Lagrangian points and Eulerian grids could be achieved through the Dirac delta function. Then we can get the functions of the force spread into the Eulerian grids, flow field and velocity of the points on the immersed boundary.

When the Direct forcing is exerted by  $NF$  times in a time step, the velocity at the immersed boundary can get close enough to the desired velocity under the no-slip condition. The interaction force between fluid and Lagrangian points could be described as :

$$\mathbf{F}_k(\mathbf{x}_k) = \sum_{i=1}^{NF} \mathbf{F}_k^i(\mathbf{x}_k). \quad (7)$$

The method mentioned above is called Multi-direct Forcing (Luo et al., 2007); (Wang et al., 2008).

A closed-form expression for the velocity distribution over a smooth wall is valid continuously from the wall up to the freestream (Musker, 1979). In this paper, it is applied to calculate the streamwise velocity of the entrance velocity. And the open boundary condition (Orlanski, 1976) is applied as the convective velocity boundary condition.

### 2.3 Computational Domain

The geometrical parameters of the domain are  $X \times Y \times Z = 74.55\text{mm} \times 14.1\text{mm} \times 10.5\text{mm}$ , which can be seen in figure1, and the sphere center is placed at  $O(16.35\text{mm}, 7.05\text{mm}, 1.8\text{mm})$ . The precision of uniform grid is  $50\mu\text{m}$ , thus the grid amount of the whole flow field is 92,897,280. The domain is divided into 48 subdomains, and the resolution along the streamwise, spanwise and wall-normal directions are  $16 \times 3 \times 1$ . Parameters of the sphere and fluid are

set out in Table 1.

The size of the gap between the bottom of the sphere and the plane is 0.1D, which is 0.3mm. According to the expression  $N_L \geq \frac{\pi}{3} \left( 12 \frac{r_c^2}{h^2} + 1 \right)$ , the amount of Lagrangian points (Uhlmann, 2005) is 9520, distances between any two points are equal in length.

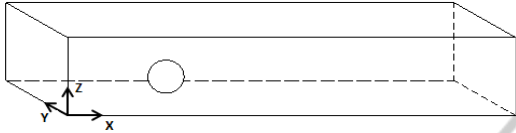


Figure 1: Schematic view of the computational domain.

Table 1: Summary of prediction conditions.

Parameter	value
Sphere diameter, D (mm)	3
Position of the sphere center, O(x <sub>o</sub> ,mm,y <sub>o</sub> ,mm,z <sub>o</sub> ,mm)	(16.35 , 7.05 , 1.8)
Air density, ρ(kg/m <sup>3</sup> )	1.205
Air viscosity, μ (kg/m/s)	1.82×10 <sup>-5</sup>
Free stream velocity, U (m/s)	21

### 3 RESULTS AND DISCUSSION

According to the simulation results, we analyse the structure of the vortex, the distribution of velocity and pressure, the turbulence intensity, and so on.

The structure of the vortex is observed in figure 2, from which no horseshoe vortices and arch vortices could be find, but hairpin vortex formed and shed form the sphere, thus the forest vortices are formed. It is consistent with the experimental results of Takayuki (Takayuki, 2008).

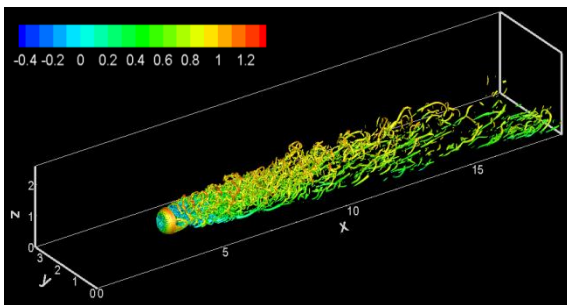


Figure 2: Vortex structure of the entire domain.

The average velocity field in the center section  $Y=y_o$  at four different time steps are presented in figure 3. The streamwise velocity distribution of the boundary layer is visualized clearly. It can be seen from the illustration that there is a typical laminar

flow velocity distribution in front of the sphere. Then the flow is splited: the under part flows through the gap between the sphere and the plane. Because of the across area reducing suddenly, a high velocity area is formed, extending to the recirculation region behind the sphere. And the upper part climbs upward along the sphere. Boundary layer separation take place on the separation point at the top of the sphere. The separated boundary layer sharply thickens along the flow, and under the separated boundary layer, a recirculation region is formed behind the sphere. The sharply thickening of the boundary layer indicates the transition of the boundary layer. And behind the transition zone, the profile of the boundary layer velocity converts from the fully developed laminar boundary layer to fully developed turbulent boundary layer. According to figure 3, the turbulent boundary layer develops continuously with time, and the wake rises along the normal direction. At the same time, the length of the transition zone reduces. Laminar sublayer could be distinguished from figure 3(c).

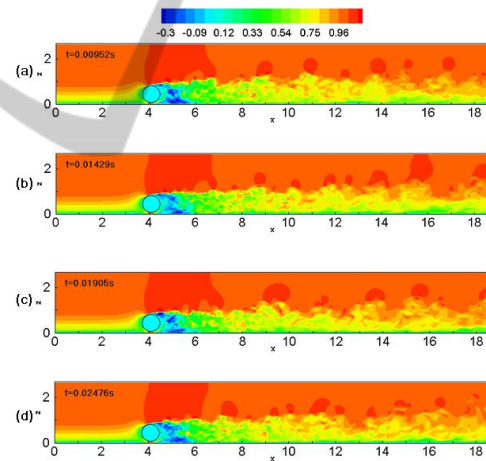


Figure 3: The streamwise velocity distribution of the boundary layer, (a)  $t=0.00962s$ , (b)  $t=0.01429s$ , (c)  $t=0.01905s$ , (d)  $t=0.02476s$ .

Figure 4(a) shows the profiles of the mean velocity defect at  $X/D=10(X=x-x_o)$ . With the vertical distance increasing, the peak velocity defect decreases and almost vanishes at  $Z/D=0.8$ . And as the upward distance increasing, its position closed to the center when  $Z/D < 0.6$ , yet moved away from the center when  $Z/D > 0.6$ . On the spanwise direction, the velocity defect decreases faster when  $Y/D > 0.5(Y=y-y_o)$  than the center behind the sphere. Figure 4(b) indicates the mean velocity defect at  $Z/D=0.6$ . In the range of  $Y/D < 0.7$ , the peak defect is

mainly affected by the recirculation region behind the sphere. When the downstream distance increasing, the center peak defect decreases, and another peak velocity defect appears at  $X/D=7$ . The spanwise peak defect shifts in the  $Y$ -direction, which takes place at  $Y/D=1.1$  for  $X/D=7$  and at  $Y/D=1.4$  for  $X/D=14$ . Figure 5(a)-(f) shows the profile of mean velocity at plane  $Y=y_0$ .

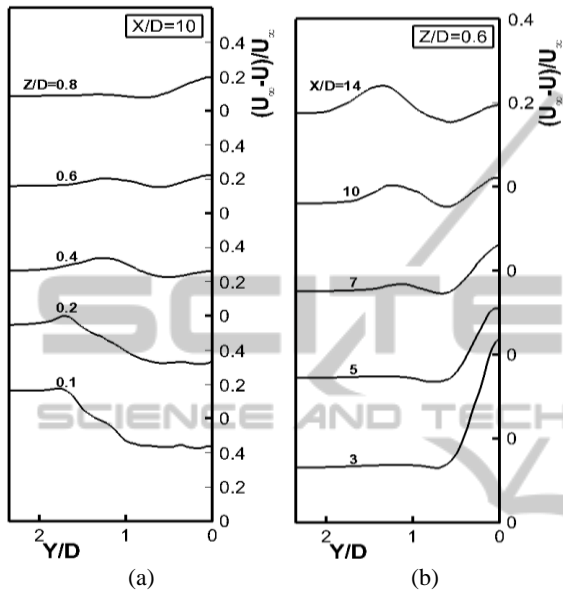


Figure 4: (a) Profiles of mean velocity defect in the vertical section  $X/D=10$ ; (b) Profiles of mean velocity defects in the horizontal centre section  $Z/D=0.6$ .

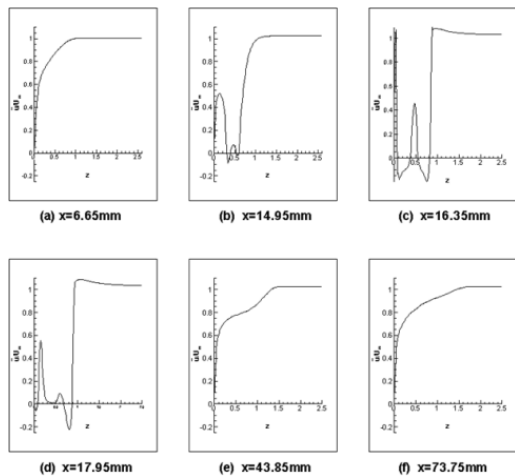


Figure 5: Profiles of mean velocity in the centre section  $Y=y_0$ . (a)  $x=6.65$ mm, (b)  $x=14.95$ mm, (c) $x=16.35$ mm, (d) $x=17.95$ , (e)  $x=43.85$ mm, (f)  $x=73.75$ mm.

The dimensionless position of the sphere center at  $Z$ -axis is 0.075. At  $x=6.65$ mm, a typical laminar boundary layer velocity profile is presented as the

entrance velocity profile. In figure 5(b) fluctuations in the range of  $0.3 < z < 0.6$ , is the result of the IBM method, not the velocity of fluid. According to the IBM method, it is solid inside the sphere, which has been computed as fluid. Thus the velocity is 0 in fact. And the profile indicates that the existence of the sphere “breaks” the laminar boundary layer velocity profile. The mean velocity profile at the position of the sphere center is observed in figure 5(c). Actually, the fluctuation in the range of  $0.075 < z < 0.825$  is not the velocity of fluid as well. Due to the influence of the sphere, a high velocity area forms in the gap between the sphere and the plane. In the range of  $0.825 < z < 1.000$  at the top of the sphere, a thin boundary layer exists, where the dimensionless velocity sharply increases from 0 to 1.2. Figure 5(d) shows the mean velocity profile at 0.1mm behind the sphere. Because of separation of the boundary layer and the formation of the recirculation region, mean velocity presents negative values. Figure 5(e) and (f) respectively describes the profile at  $x=43.84$ mm and  $x=73.75$ mm. The influence of the sphere on the boundary layer is much weaker when  $x$  equals to 73.75mm, and the velocity profile indicates a typical turbulent layer velocity profile.

The pressure distribution on the plane can be observed in figure 6. There are two areas of high pressure respectively in front of the sphere and behind the recirculation area. Behind the sphere, the low pressure area which coincides with the recirculation area is reduced rapidly because of a strong downwash behind the sphere. Hence the length of the recirculation region is considered to be twice as much as the diameter of the sphere between the two high pressure areas.

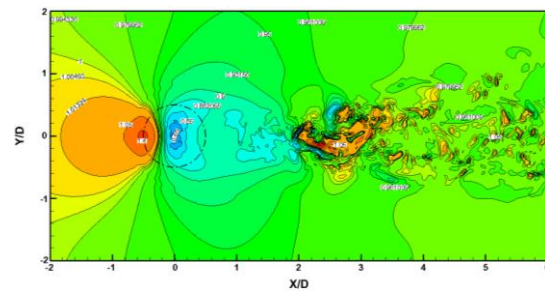


Figure 6: The pressure distribution on the plane.

In figure 7 the time-mean velocity profiles at  $X/D=5 \sim 14$  are presented. The thickness of boundary layer is nearly equal to  $1.8D$  at  $X/D=5$ , and thickens with downstream distance increasing. The turbulence intensity on  $X$ -component,  $Y$ -component and  $Z$ -component are compared in figures 8-10. Because of the existence of the sphere, the

turbulence intensity values in the vertical direction is divided into three zones naturally. In the range of  $0 < z < 0.075$ , turbulence intensity in X-direction and Y-direction decreases rapidly with the vertical distance increasing, but in Z-direction, it increases. In the range of  $0.075 < z < 0.825$ , turbulence intensity is about 0.1 in all directions and decreases with streamwise distance increasing. The value of turbulence intensity gradually tends to the value of freestream in the range of  $z > 0.825$ , which approaches zero. And the change is gentler as the streamwise distance increasing. Thus it can be seen that turbulence intensity is increase in the shear layer.

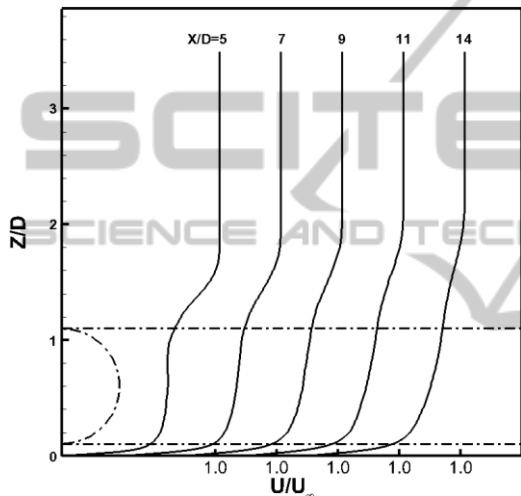


Figure 7: Profiles of mean velocity in the centre section  $Y=y_0$ .

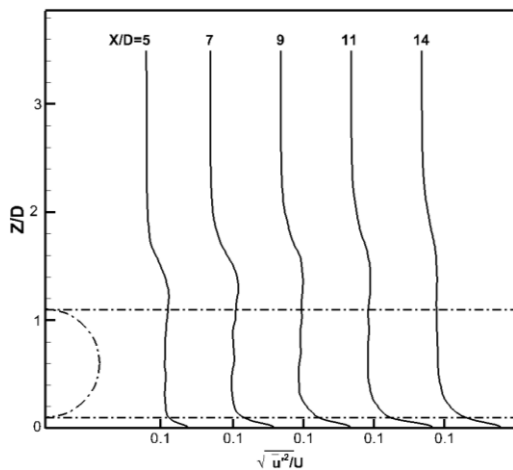


Figure 8: Profiles of turbulence intensity in X-direction in centre section  $Y=y_0$ .

Figure 11 shows the Reynolds stresses profile in the plane  $Y=y_0$ . At the position  $x=20.60\text{mm}$ , two peaks

which have different direction are presented respectively at  $z=1\text{mm}$  and  $z=3.6\text{mm}$ . Similarly, at other positions in the X-direction, two peaks in the opposite direction exist. And with the increase of  $x$ , peak values reduce, which is closed to zero near the outlet of the computational domain where  $x$  equals to  $73.75\text{mm}$ .

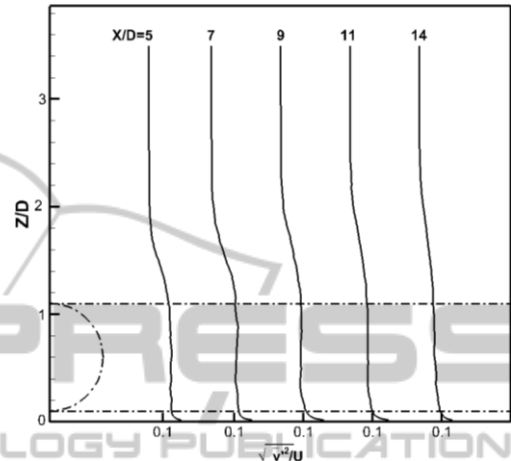


Figure 9: Profiles of turbulence intensity in Y-direction in centre section  $Y=y_0$ .

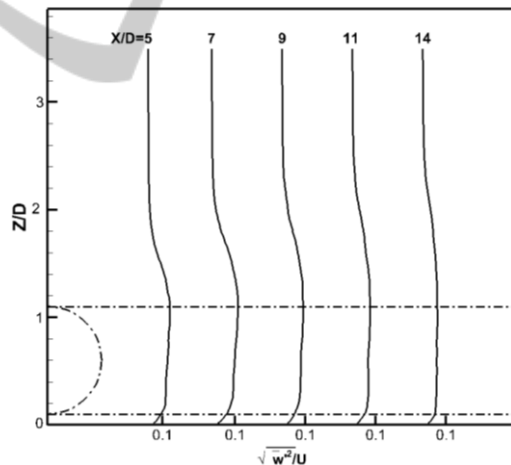


Figure 10: Profiles of turbulence intensity in Z-direction in centre section  $Y=y_0$ .

The X-component, Y-component and Z-component of the turbulence intensity in the horizontal center section ( $Z/D=0.6$ ) and the vertical section where  $X/D=10$  are shown in figures 12-13. The position of peak of turbulence intensity moves in a manner similar to peak velocity defect. While  $Z/D < 0.8$ , the turbulence intensity at the streamwise is larger than the lateral and vertical turbulence intensities. And at  $Z/D=1.2$ , the turbulence becomes almost isotropic.

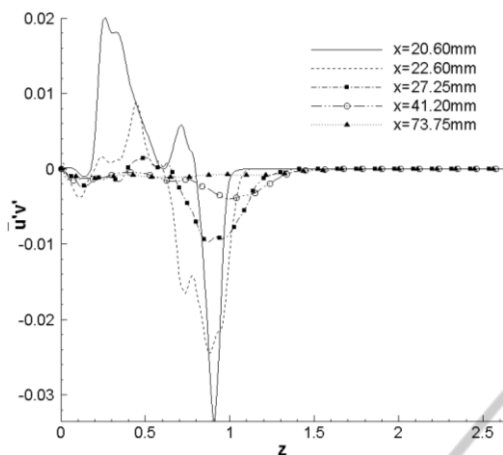


Figure 11: Profiles of Reynolds stress in the centre section  $Y=y_0$ .

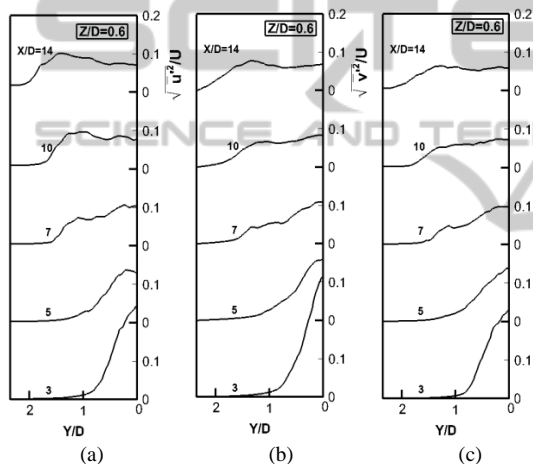


Figure 12: Profiles of turbulence intensity in the horizontal centre section ( $Z/D=0.6$ ). (a) in X-direction; (b) in Y-direction; (c) in Z-direction.

## 4 CONCLUSIONS

In this paper, we have studied the flow field around a sphere placed above a ground plane. The gap between the sphere and the plane is  $0.1D$ . The Reynolds number based on  $D$  is 4171. The MDF/IBM method has been used to deal with the coupling between fluid and solid. The main findings of this study are summarized in the following.

- (1) Hairpin vortex is formed and sheds behind the sphere, and the forest vortices are formed.
- (2) In front of the sphere there is a typical laminar flow velocity distribution. And near the outlet of the domain, the velocity distribution has turned to a typical turbulent layer velocity profile.

(3) The flow is split when flowing around the sphere: the under part forms a high velocity area and the upper part climbs upward, extending to the recirculation region behind the sphere. Boundary layer separation takes place on the separation point at the top of the sphere.

(4) A recirculation region is formed because of the strong downwash behind the sphere. The length of the recirculation region is twice as much as the sphere diameter.

(5) With streamwise distance increasing, the influence of the sphere on the boundary layer decreases. The thickness of boundary layer increases, the center peak defect and the turbulence intensity decreases. In addition the Reynolds stresses reduce, which is close to zero near the outlet of the computational domain.

With the vertical distance increasing, the peak velocity defect decreases and its position is close to the center when  $Z/D < 0.6$ , yet moves away from the center when  $Z/D > 0.6$ . The position of peak turbulence intensity peak moves in a manner similar to peak velocity defect.

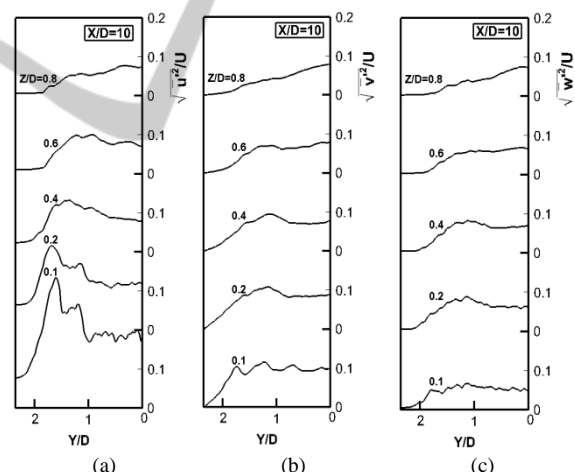


Figure 13: Profiles of turbulence intensity at  $X/D=10$ . (a) in X-direction; (b) in Y-direction; (c) in Z-direction.

## ACKNOWLEDGEMENTS

This work is supported by The National Natural Science Foundation of China (No. 51136006). We are grateful to that.

## REFERENCES

- A. J. Musker, 1979. Explicit expression for the smooth

- wall velocity distribution in a turbulent boundary layer. *AIAA Journal*, 17, 655-657.
- A. Klemm, E. B. Schaefer and J. G. Beerer, 1939. Aerodynamics of the Perisphere and Trylon at World's Fair. *Trans. Am. Soc. Civ. Eng.*, 2042, 1449-1472.
- H. Schlichting, 1939. Experimentelle untersuchungen zum ranhigkeitsproblem. *Ing. Arch.*, 7, 1-34.
- J. Mohd-Yusof, 1997. Combined immersed boundaries/B-splines methods for simulations of flows in complex geometries. *CTR annual research briefs*, 317-327.
- K. Luo, Z. Wang, J. Fan and K. Cen, 2007. Full-scale solutions to particle-laden flows: Multidirect forcing and immersed boundary method. *Physical Review E*, 76, 066709.
- L. Zeng, S. Balachandar, P. Fischer and F. Najjar, 2008. Interactions of a stationary finite-sized particle with wall turbulence. *Journal of Fluid Mechanics*, 594, 271-305.
- Orlanski, 1976. A simple boundary condition for unbounded hyperbolic flows. *Journal of Computational Physics*, 21, 251-269.
- S. Okamoto, 1980. Turbulent shear flow behind a sphere placed on a plane boundary. *Turbulent Shear Flows*, 2, 246-256.
- Tsutsui Takayuki, 2008. Flow around a sphere in a plane turbulent boundary layer. *Journal of Wind Engineering and Industrial Aerodynamics*, 96, 779-792.
- Uhlmann, 2005. An immersed boundary method with direct forcing for the simulation of particulate flows. *Journal of Computational Physics*, 209, 448-476.
- Z. Zhou, Z. L. Wang & J. R. Fan, 2010. Direct numerical simulation of the transitional boundary-layer flow induced by an isolated hemispherical roughness element. *Computer Methods in Applied Mechanics and Engineering*, 199, 1573-1582.
- Zeli Wang, Jianren Fan and Kun Luo, 2008. Combined multi-direct forcing and immersed boundary method for simulating flows with moving particles. *International Journal of Multiphase Flow*, 34, 283-302.